JOINT INSTITUTE FOR NUCLEAR RESEARCH
Dzhelepov Laboratory of Nuclear Problems

**FINAL REPORT ON THE
START PROGRAMME**

Investigation of photoneuclear reactions in the ^{165}Ho nucleus

Supervisor:
Dr.Khushvaktov Jurabek. H.

Student:
Kuyliyev Fayzullo
NRNU MEPhI

Participation period:
August 24 – October 18,
Summer Session 2025

Dubna, 2025

Content

Abstract

In this study, accelerated electron beams were directed at a lead converter with thicknesses of 3 mm and 5 mm, causing the electrons to slow down and produce bremsstrahlung γ-rays. These γ-rays then irradiate a holmium (Ho) sample placed behind the converter, inducing various photonuclear reactions in the ^{165}Ho nuclei. The aim of the study is to calculate the **relative reaction yields** and **flux-averaged cross sections** of these photonuclear reactions and to compare them with experimental results. These processes were modeled using the **Geant4** software package, and the photon flux was calculated. The electron beam energies ranged from 50 MeV to 110 MeV.

Introduction

The study of photonuclear reactions is of great importance in nuclear physics and energy research. Currently, photonuclear reactions are being investigated to study various problems, such as the mechanism of formation of produced nuclei (e.g.,^{74}Se, ^{78}Kr, ^{84}Sr, ^{92}Mo, ^{96}Ru), the influence of the isospin effect on the splitting of the giant dipole resonance, multinucleon photonuclear reactions with up to ten nucleons emitted, photofission of actinide nuclei (U, Th), and isomeric ratios in photonuclear reactions [5]. Photonuclear reactions occur when gamma rays interact with nuclei, causing one or more nucleons to be emitted. These processes are most active in the giant dipole resonance (GDR) energy range.

A detailed study of photonuclear reactions allows the solution of several important problems, such as the production of radioisotopes for nuclear medicine, safe energy generation, and transmutation of radioactive waste. For practical applications, **accelerator-driven subcritical assemblies (ADS)** serve as a promising solution. In subcritical systems, chain reactions do not continue independently but are controlled by an external neutron source (accelerator), which provides a high level of safety.

Currently, several neutron sources based on linear electron accelerators with energies up to 200 MeV exist worldwide, including **IREN** (JINR, Dubna, Russia) [1], **GELINA** (JRC, Geel, Belgium) [2], and **ORELA** (ORNL, Oak Ridge, USA) [3]. Linear electron accelerators, such as the **LINAC-200** at the Joint Institute for Nuclear Research in Dubna, serve as effective sources of bremsstrahlung gamma rays to induce photonuclear reactions [4]. Such studies provide valuable information about the reactions occurring in various nuclei and their physical characteristics.

The **LINAC-200** is currently capable of accelerating electron beams with energies from 20 to 200 MeV, with plans to increase the energy to 2 GeV in the future [4]. Bremsstrahlung gamma rays are produced by irradiating a lead converter with the electron beam. Multinucleon photonuclear reactions—where gamma rays cause the emission of several nucleons from a nucleus—are also an important topic of study. In this research, **holmium (Ho) samples** were chosen because photonuclear reactions with up to ten nucleons emitted can occur in these nuclei [4].

When electron beams from the LINAC-200 hit the lead converter, two main types of radiation are produced: a broad-spectrum **gamma-ray flux (bremsstrahlung)** as the primary component and a **neutron flux** as a secondary, less abundant component. Since the main reactions of interest are photonuclear reactions induced by gamma rays, the study focused primarily on the gamma flux.

In this work, the photonuclear reactions occurring in ^{165}Ho were analyzed. Their **relative reaction yields** and **flux-averaged cross sections** were calculated, and the processes were modeled using the **Geant4 software package**, allowing the photon flux to be determined. The simulation results were then compared with available experimental data.

Research methods

2.1. Calculation Methodology and Software Packages Used (Geant4 and TALYS)

In this study, the following processes were modeled using the **Geant4** software package: accelerated electron beams were directed at a lead (Pb) converter, and as the electrons slowed down, bremsstrahlung γ-rays were produced. These γ-rays then irradiated the ^{165}Ho nuclei placed behind the converter, inducing various photonuclear reactions. The aim of the study was to calculate the **relative reaction yields** and **flux-averaged cross sections** of these photonuclear reactions. The effects of **electron energy** and **converter thickness** on the results were presented graphically and compared with experimental data.

Regarding the calculation methodology, **Geant4** was used to model the interaction of particles with matter, while **TALYS**, a theoretical nuclear reaction code, was employed to calculate the cross sections of the reaction channels produced in ^{165}Ho nuclei. Additionally, for the reaction ^{165}Ho(γ,7n2p)^{156}Tb, the reaction cross sections of the produced ^{156}Tb were calculated separately in both Geant4 and TALYS. The relative reaction yields were determined, presented graphically, and the results obtained from **experiment, Geant4, and TALYS** were compared with each other.

Geant4 software package

Geant4 (from **Geometry and Tracking**) [6] is a software package designed to model the passage of elementary particles through matter using Monte Carlo methods. It was developed by the **Geant4 Collaboration** (CERN and other institutes) in an object-oriented **C++ programming language** [6]. The first releases appeared in 1998. Geant4 is the advanced

and significantly upgraded continuation of previous GEANT versions. The earlier versions 1, 2, and 3 were written in Fortran.

According to the official project website, the application areas include **high-energy physics, nuclear reaction studies, medicine, particle accelerators, and space physics research**. Geant4 allows modeling of particles with energies ranging from a few eV up to GeV [6]. The software is used in numerous research projects worldwide, including Russia. The primary operating environment for Geant4 is **Scientific Linux**, though it is also compatible with other Linux distributions and Microsoft Windows. The initial source code of Geant4 was open to the public, and a specific license confirming its open-source status—the **Geant4 Software License**—was issued with version 8.1 on June 30, 2006 [6].

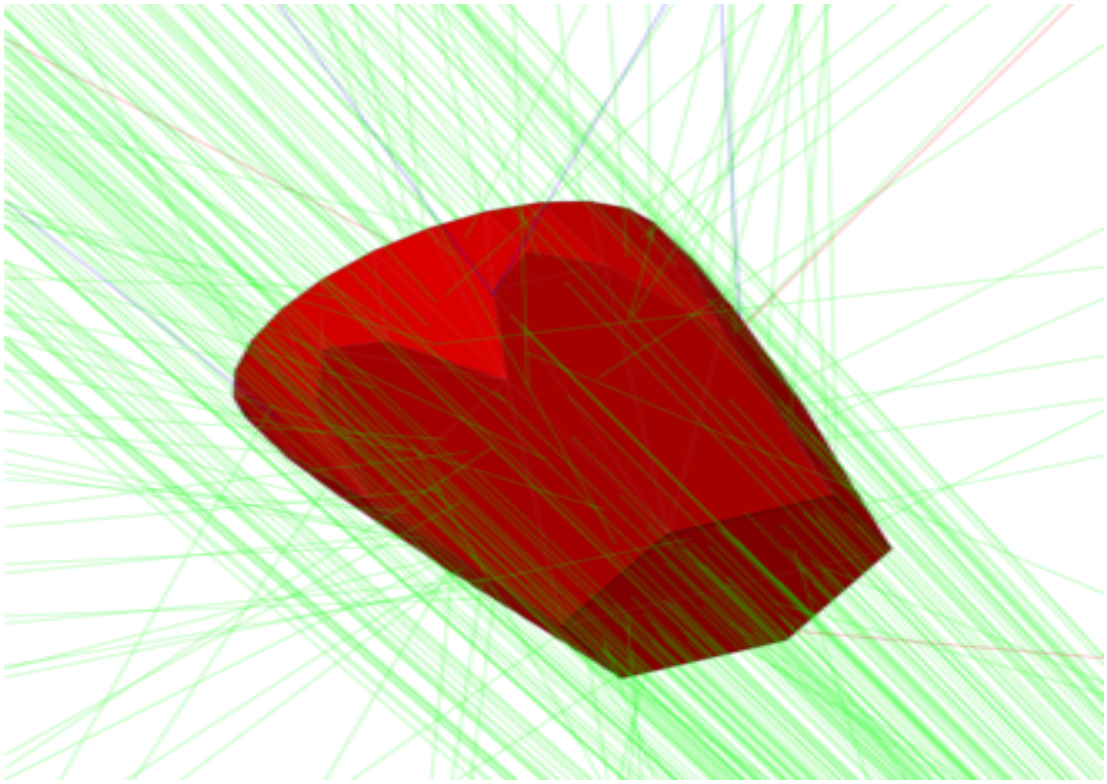

Fig. 1. Example of visualization — a detector irradiated by a gamma-ray beam directed along the axis. The detector is shown in red. Green lines represent the trajectories of gamma photons, red lines indicate electrons, and blue lines show positrons [6].

TALYS

TALYS is a nuclear reaction calculation software. It is used to calculate the cross sections σ(E) of reactions when various particles (n, p, d, t, ^{3}He, α, γ) hit a target nucleus, as well as to model the resulting spectra, angular distributions, and the production of residual isotopes (activation).

It is used in nuclear physics for the following purposes:

1. **Data evaluation (TENDL).** Experimental data on nuclear reactions are not always complete. Codes like TALYS use theoretical models to calculate **cross sections (σ),** output spectra, and other quantities, filling gaps in data libraries (e.g., TENDL) and smoothing discrepancies to create a consistent and reliable dataset.
2. **Activation and radiation safety.** TALYS allows the prediction of which residual nuclei will be produced in a target under irradiation, their half-lives, and isomeric ratios. This helps in assessing activity in laboratory or industrial settings, planning measurement spectra in advance, and choosing appropriate safety measures (such as shielding and exposure time).
3. **Reactor/ADS and shielding (neutron–gamma fields).** In reactors or ADS systems, it is important to know the distribution of neutron and gamma fluxes within materials and how the corresponding cross sections vary. These calculations enable more accurate shielding design, material selection, and dose assessment.
4. **Production of medical isotopes.** TALYS allows the calculation of which targets and reactions can produce the desired medical radioisotopes most efficiently and cleanly (for example, at which energies the yield is highest and unwanted by-products are minimized). This helps optimize production pathways.

5. **Astrophysics (reactions inside stars).** Nuclear fusion and other reactions occurring inside stars cannot be fully measured directly in the laboratory. Using models, cross sections and reaction rates are estimated, allowing theoretical scenarios of element formation (nucleosynthesis) and stellar evolution to be tested.

In the conducted experiment, electron beams were accelerated using the **LINAC-200** accelerator to energies of 60, 80, and 100 MeV. A lead (Pb) converter with a thickness of 3 mm was used for the 60 MeV beam, and a 5 mm thick converter was used for the 80 MeV and 100 MeV beams. In our study, during the **Geant4** modeling, the electron beam energies were varied from 50 MeV to 110 MeV in 5 MeV steps, and separate simulations were performed for the 3 mm and 5 mm lead converters. In the experiment, the **holmium (Ho) sample** had a mass of 500 mg.

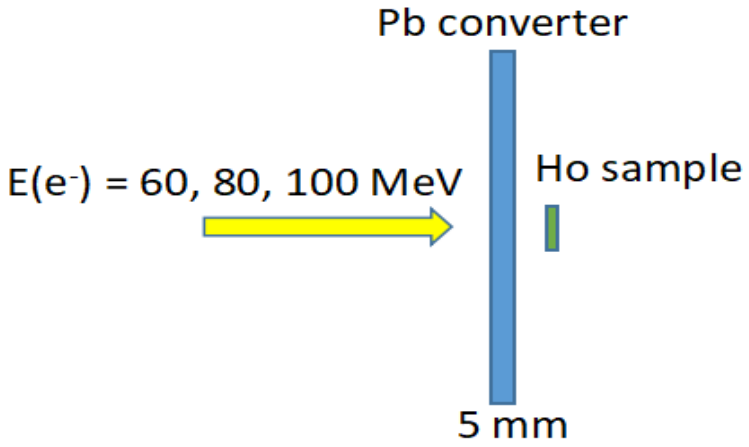

Fig. 2. Experimental setup.

R (reaction yield) – the number of nuclei produced per unit time per target atom or per incident electron.

$$R = N_t \cdot \Phi \cdot \langle\sigma\rangle$$

R – reaction yield (number of reactions per second);

N_t- number of target nuclei.

Φ - incident particle flux $(\frac{1}{sm^2 \cdot c})$

$\langle\sigma\rangle$– reaction cross section (sm^2or barn)

The flux-average cross section ($\langle\sigma\rangle$) is often used because gamma radiation has a spectral distribution.

$$\langle\sigma\rangle = \frac{\int \sigma(E)\cdot\Phi_\gamma dE}{\int \Phi_\gamma dE}$$

Reaction cross section (σ) – the probability that a reaction will occur when a single particle (e.g., a gamma photon) collides with a target nucleus.

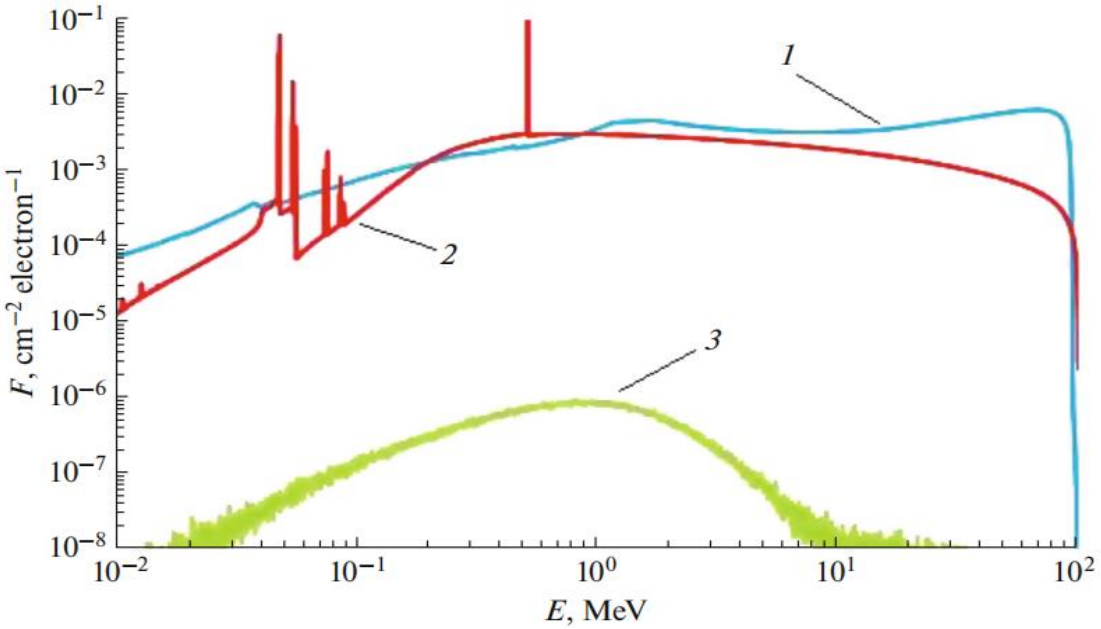

Fig. 3. Dependence of the *F* fluence of electrons (*1*), photons (*2*) and neutrons (*3*) on their *E* energy [4].

On the horizontal X-axis, **E – energy (MeV)** is plotted. On the vertical Y-axis, **F – fluence**, i.e., the number of particles per incident electron, is shown. When electrons enter the Pb converter, they lose energy through **ionization losses, multiple scattering, and bremsstrahlung radiation**. The resulting γ-photons can then produce **electron-positron pairs (pair production)**. This sequence of processes is called an **electromagnetic shower**. In the shower, a large number of secondary electrons are generated. Therefore, at low to medium energies, the number of electrons (fluence) appears higher. At the high-energy end of the spectrum, there is a sharp drop: near $E \rightarrow E_0$ (the initial energy of the incident electrons),

almost no electrons remain, as most of them have lost energy inside the converter due to radiation and ionization. This is why the blue line terminates at the “endpoint” at high energy. This electromagnetic shower generates the **bremsstrahlung γ-spectrum** (red line, $\Phi_\gamma(E)$). Thus, the blue line illustrates how the electron beam “breaks up” and transforms into many low-energy secondary particles, which subsequently form the $\Phi_\gamma(E)$ used in photonuclear reaction calculations. The red line represents the bremsstrahlung photon spectrum. High-energy electrons decelerate strongly in the Coulomb field of the Pb converter, producing bremsstrahlung γ-radiation. As a result, a broad and decreasing spectrum is formed. The green line shows the spectrum of secondary neutrons.

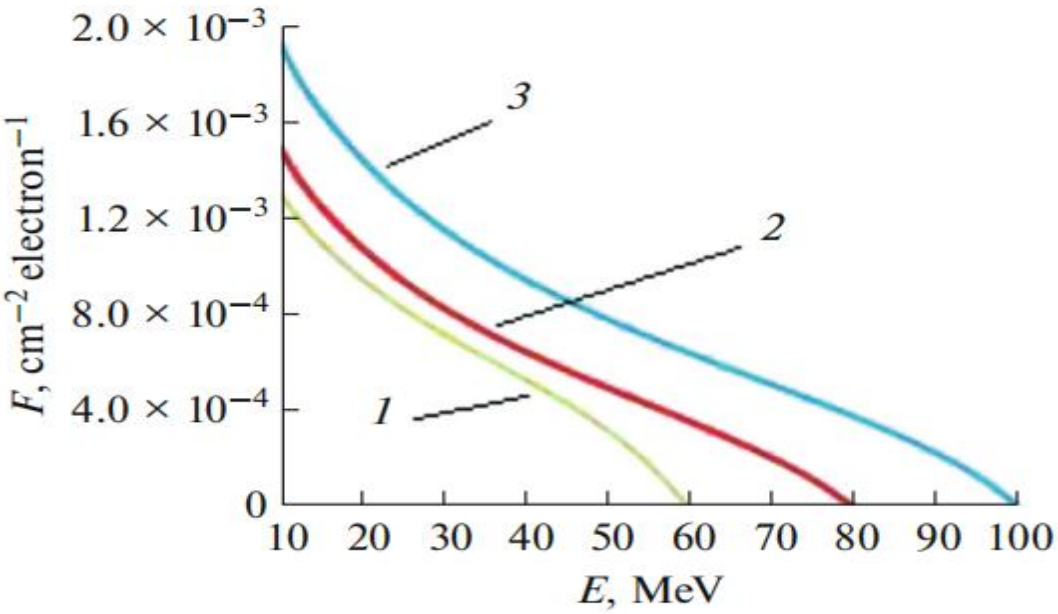

Fig. 4. Energy spectrum of bremsstrahlung for electrons with energies of 60 (*1*), 80 (*2*) and 100 (*3*) MeV [4].

On the horizontal X-axis, **E (MeV)** represents the photon energy. On the vertical Y-axis, **F** denotes the photon fluence, i.e., the number of photons per incident electron.

1 - $E_e = 60\ MeV$, 2 - $E_e = 80\ MeV$ va 3 - $E_e = 100\ MeV$ correspond to the bremsstrahlung spectra for these electron energies. In all cases, the

spectra are decreasing. At low to medium energies, there are many photons, while the number approaches zero as E_γ approaches the electron energy (endpoint = E_e). As the electron energy increases, the fluence rises across the entire spectrum.

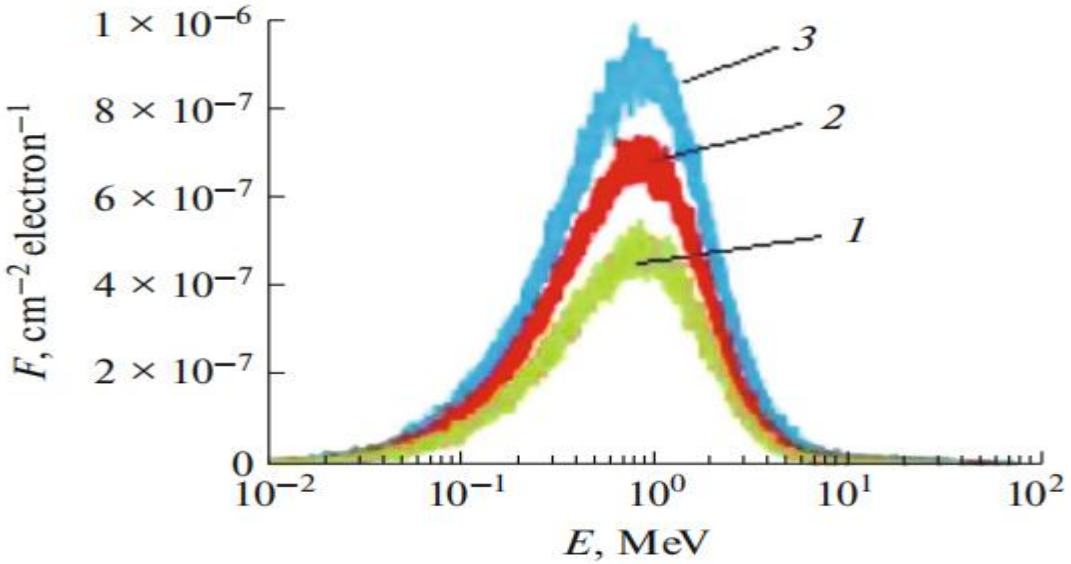

Fig. 5. Energy spectrum of secondary neutrons for electrons with energies of 60 (*1*), 80 (*2*) and 100 (*3*) MeV [4].

On the horizontal X-axis, **E (MeV)** represents neutron energy. On the vertical Y-axis, **F** shows the neutron fluence. The peak is around ≈ 0.5–1 MeV, then it decreases rapidly at higher energies. These neutrons are produced in the Pb converter as a result of photonuclear processes induced by bremsstrahlung γ-rays. As the electron energy E_e increases (1 → 2 → 3), the fluence rises across the entire spectrum, with higher electron energies producing more neutrons. These neutrons can induce (n,γ) and other neutron-induced background reactions in the Ho sample, which must be taken into account in activation analysis.

Bremsstrahlung radiation

Bremsstrahlung (from the German *bremsen* "to brake" and *Strahlung* "radiation"; i.e., "braking radiation" or "deceleration radiation") is **electromagnetic radiation produced when a charged particle,**

usually an electron, is deflected by an atomic nucleus, causing the particle to decelerate [7]. The moving particle loses kinetic energy, which is converted into a photon, thus satisfying the law of energy conservation. The term also refers to the process of generating this radiation. Bremsstrahlung has a **continuous spectrum**, which intensifies and shifts to higher frequencies as the energy of the decelerating particle changes. The **maximum radiation frequency** is related to the kinetic energy of the electrons [7].

$$E = h \cdot \nu_{max} \quad (1)$$

The minimum wavelength of the emitted radiation is given by [7]:

$$\lambda_{min} = \frac{c}{\nu_{max}} = \frac{hc}{E} \quad (2)$$

In general, **bremsstrahlung** or braking radiation refers to any radiation produced by the deceleration (negative acceleration) of a charged particle, which includes **synchrotron radiation** (photon emission by a relativistic particle), **cyclotron radiation** (photon emission by a non-relativistic particle), and the emission of electrons and positrons during beta decay. However, the term is often used in a narrow sense to describe the radiation produced when electrons (from any source) are decelerated in matter. According to Maxwell's equations, accelerated charges emit electromagnetic radiation. Specifically, when an electron strikes a material, it is deflected by the Coulomb field of atomic nuclei, and thus can be considered “braked.” If the energy of the bombarding electrons is sufficiently high, the emitted radiation falls within the **X-ray region** of the electromagnetic spectrum [7]. For bremsstrahlung, the energy loss is significant, dominating over ionization and nuclear excitation processes—for high-energy electrons, this can be on the order of hundreds of MeV in

air and water, and tens of MeV in heavy materials like lead or iron. The **average energy loss per unit length** can be approximately estimated as follows [7]:

$$-\left(\frac{dE}{dx}\right) \approx \frac{4N_\alpha Z^2 \alpha^3 (\hbar c)^2}{m_e^2 c^4} E \ln \frac{183}{Z^{1/3}} \qquad (3)$$

Here N_α is the number of atoms per unit volume, Z is the atomic number of the target material, **α** is the fine-structure constant, and m_e is the electron mass. Therefore, the energy loss is **proportional to** Z^2 , and inversely proportional to the particle's energy E and mass. For particles heavier than electrons, bremsstrahlung radiation is negligible.

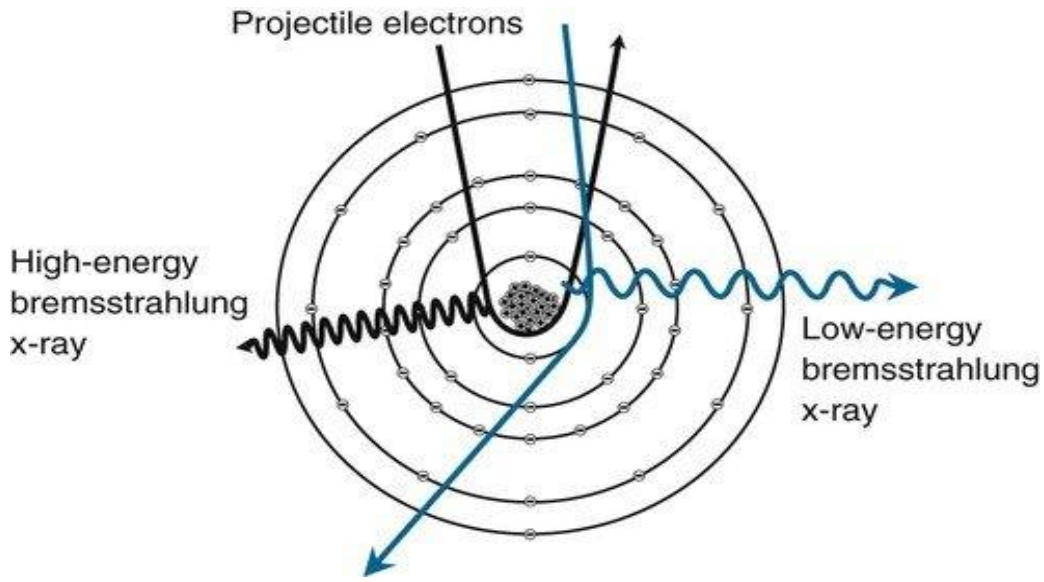

Fig. 6. Bremsstrahlung Radiation Process: Interaction of High-Energy Electrons with Atomic Electrons [7].

This continuous spectrum even includes some intense lines because the bombarding electrons can eject electrons from the innermost atomic shells of the target, and the rapid filling of these vacancies by electrons from higher shells produces **characteristic X-rays** (also called X-ray fluorescence) for each atom, as illustrated in the adjacent figure.

Additionally, the energy difference between two orbitals can lead to further ejection of electrons. This phenomenon is known as the **Auger effect**.

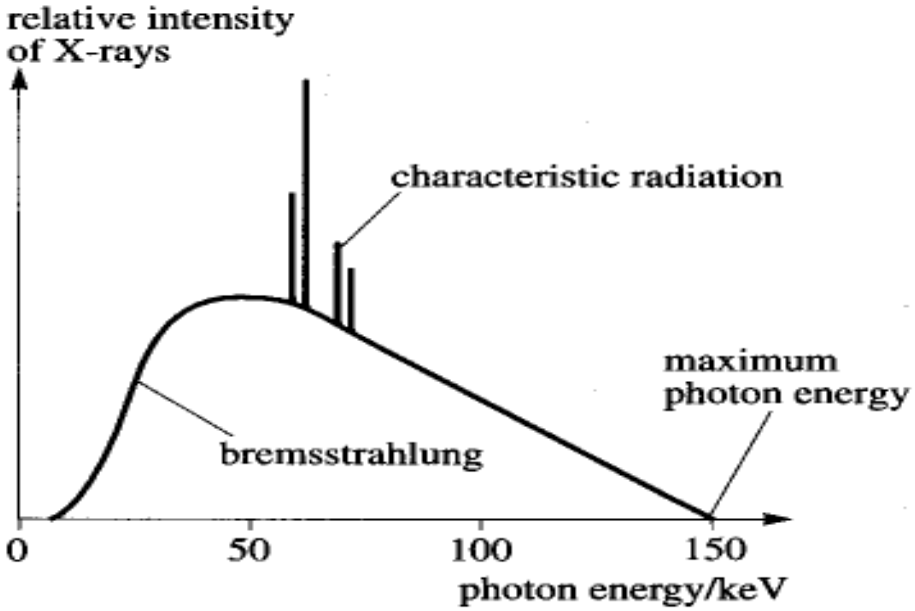

Fig. 7. X-ray Spectrum: Bremsstrahlung and Characteristic Radiation [7]

2.2. Overview of Photonuclear Reactions Produced in ^{165}Ho Nuclei

This section is introduced with this schematic figure, as it clearly shows the photon absorption regions (I–IV) and their physical characteristics at a glance. Our energy range, 50–110 MeV, corresponds to the tail of the GDR and extends to the quasi-deuteron region. In this range, the (γ,n) channel opens early, and multi-neutron and proton-emission channels increase rapidly. Therefore, the trends of the relative yields and average cross sections presented later are based on this energy map. This is why the figure serves as a "roadmap" for the section, helping to physically interpret the subsequent tables and graphs.

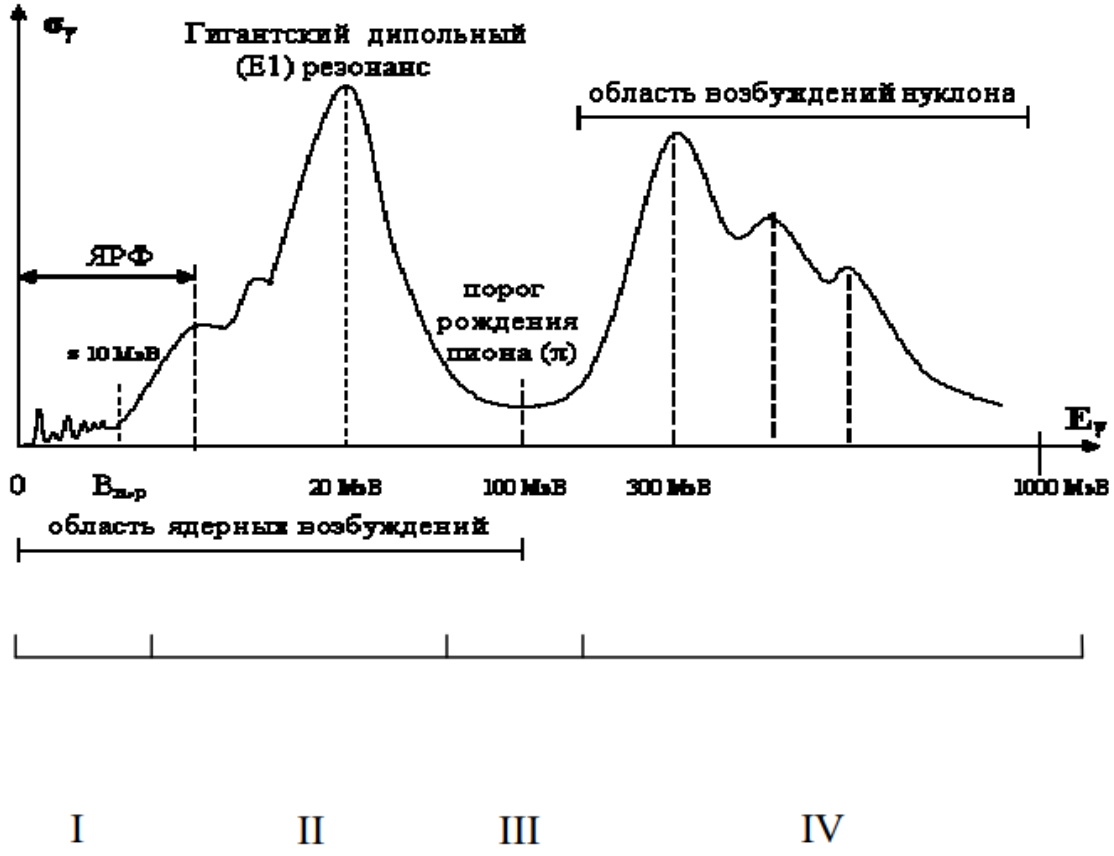

Fig. 8. Schematic representation of photon absorption cross sections by atomic nuclei in the photon energy range up to Eγ ≈ 1 GeV [8].

I — The γ-photon energy is insufficient to eject individual nucleons or small bound systems of nucleons (deuterons, α-particles, etc.) from the nucleus.

II — The absorbed photon energy is sufficient to eject one or several nucleons from the nucleus, as well as small bound systems of nucleons. In heavy nuclei, **photofission** (nuclear fission) may also occur.

III — The wavelength of the photon absorbed by the nucleus becomes smaller than the nuclear radius, and the photon mainly interacts with small bound nucleon systems formed inside the nucleus (quasi-deuteron, quasi-α-particle, etc.). In this energy region, nuclear photodisintegration typically begins with the breakup of these systems, mainly quasi-deuterons, and ends with the emission of several (even up to ten) neutrons from the nucleus.

IV — The photon wavelength becomes comparable to the size of a nucleon. The photon interacts with individual nucleons, exciting them to a resonant state.

The **relative reaction yields** and **flux-averaged cross sections** were calculated for the following photonuclear reactions occurring in ^{165}Ho nuclei:

165Ho(γ,n)164Ho, 165Ho(γ,3n)162mHo, 165Ho(γ,3n)162Ho,
165Ho(γ,4n)161Ho, 165Ho(γ,5n)160mHo, 165Ho(γ,5n)160Ho,
165Ho(γ,6n)159Ho, 165Ho(γ,3p3n)159Gd, 165Ho(γ,7n)158Ho,
165Ho(γ,8n)157Ho, 165Ho(γ,7n2p)156Tb, 165Ho(γ,9n)156Ho,
165Ho(γ,155n)155Ho.

Table 1. Threshold energies of photonuclear reactions and **half-lives of residual nuclei produced** in Ho nuclei.

Reaction channels	**Threshold energy [MeV]**	**Half life of residual nuclei**
165Ho(γ,10n)155Ho	92	48 m
165Ho(γ,9n)156Ho	82	56 m
165Ho(γ,8n)157Ho	70	12,6 m
165Ho(γ,7n)158Ho	60	11,3 m
165Ho(γ,6n)159Ho	50	33 m
165Ho(γ,5n)160Ho	42	26 m
165Ho(γ,5n)160mHo	42	5 h
165Ho(γ,4n)161Ho	30	2,5 h
165Ho(γ,3n)162Ho	22	15 m
165Ho(γ,3n)162mHo	22	67 m
165Ho(γ,n)164Ho	8	29 m

This table helps to understand the physical mechanisms of the reaction channels produced in Ho nuclei. For each photonuclear reaction, the table shows the **threshold energy** and the **half-life of the residual nucleus**.

The threshold energiyasi E_{th} indicates the minimum photon energy required for each channel, i.e., the photon energy necessary to initiate the reaction. This parameter is one of the key indicators when selecting channels and modeling reactions.

The half-life ($T_{1/2}$) indicates the stability of the residual nucleus or its probability of decay, which helps in determining experimental measurements and detector sensitivity.

This table provides the key parameters necessary for understanding the nature of the reactions and comparison results, serving as a foundation for comparing experimental and calculated data.

Additionally, for several reaction channels produced in Ho nuclei, the **energy-dependent cross sections** of the photonuclear reactions were also presented graphically using the **EXFOR** database. **EXFOR** (Experimental Nuclear Reaction Data) is a database of experimental data on nuclear reactions.

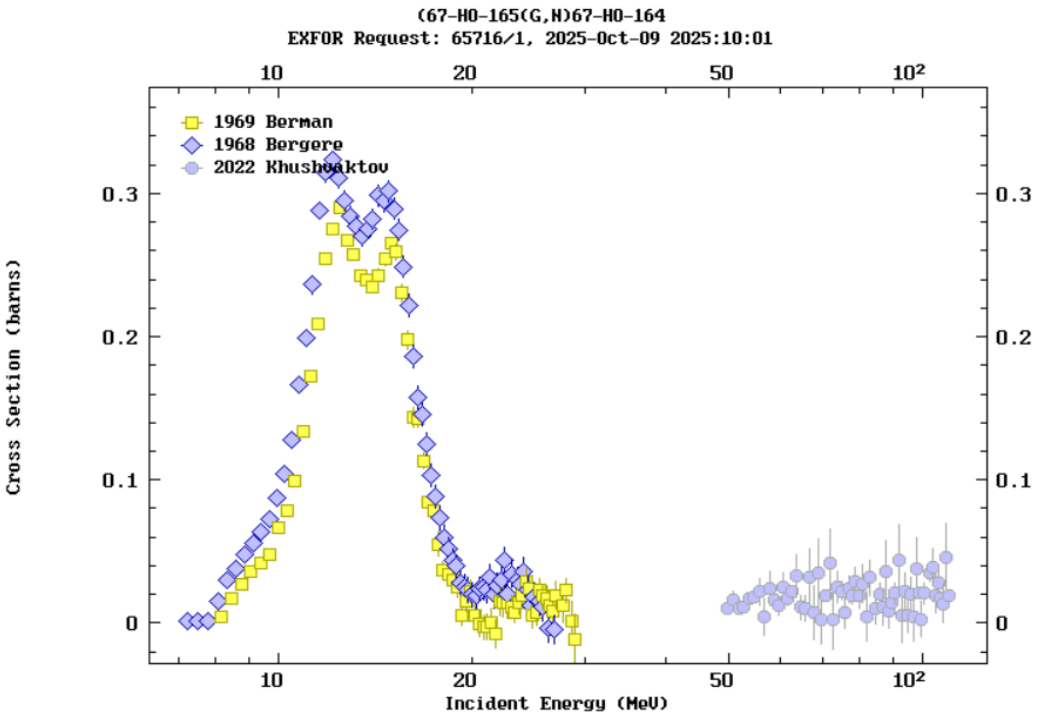

Fig. 9. EXFOR data for the ^{165}Ho(γ,n)^{164}Ho reaction. Reaction cross sections as a function of energy [5],[9],[10].

On the **X-axis (abscissa)**, the photon energy E_γ(MeV) i.e., the energy of the incident photon — is plotted.

On the **Y-axis (ordinate)**, the reaction cross section σ(E) is plotted, showing how the cross section changes as the photon energy increases.

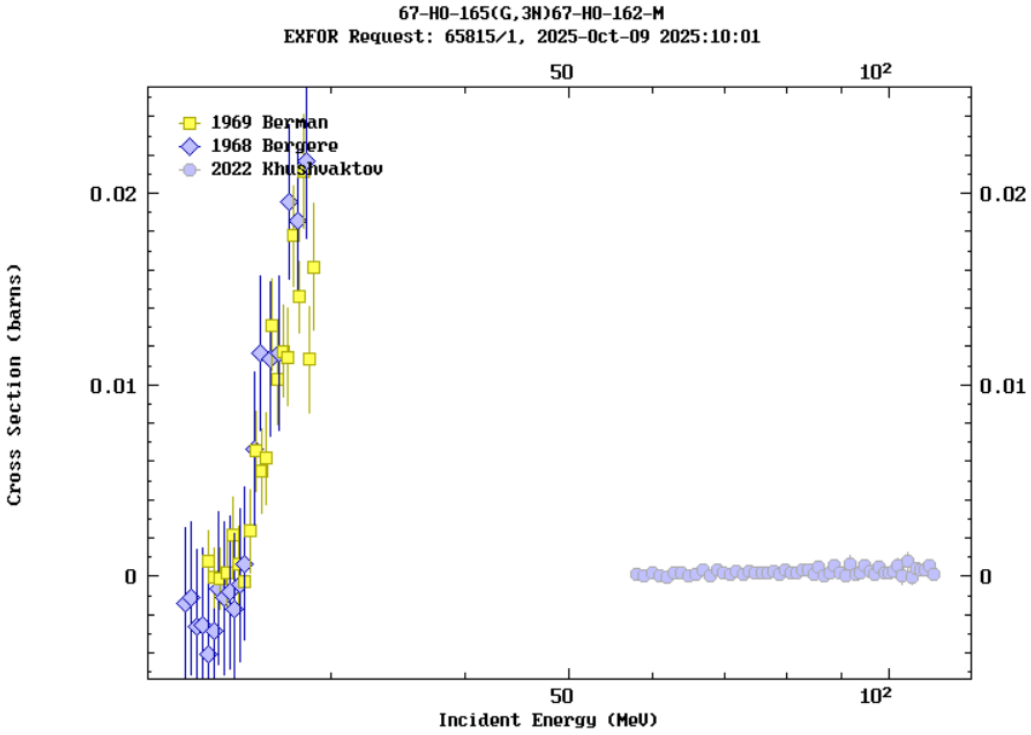

Fig. 10. EXFOR data for the 165Ho(γ,3n)162Ho reaction. Reaction cross sections as a function of energy [5],[9],[10].

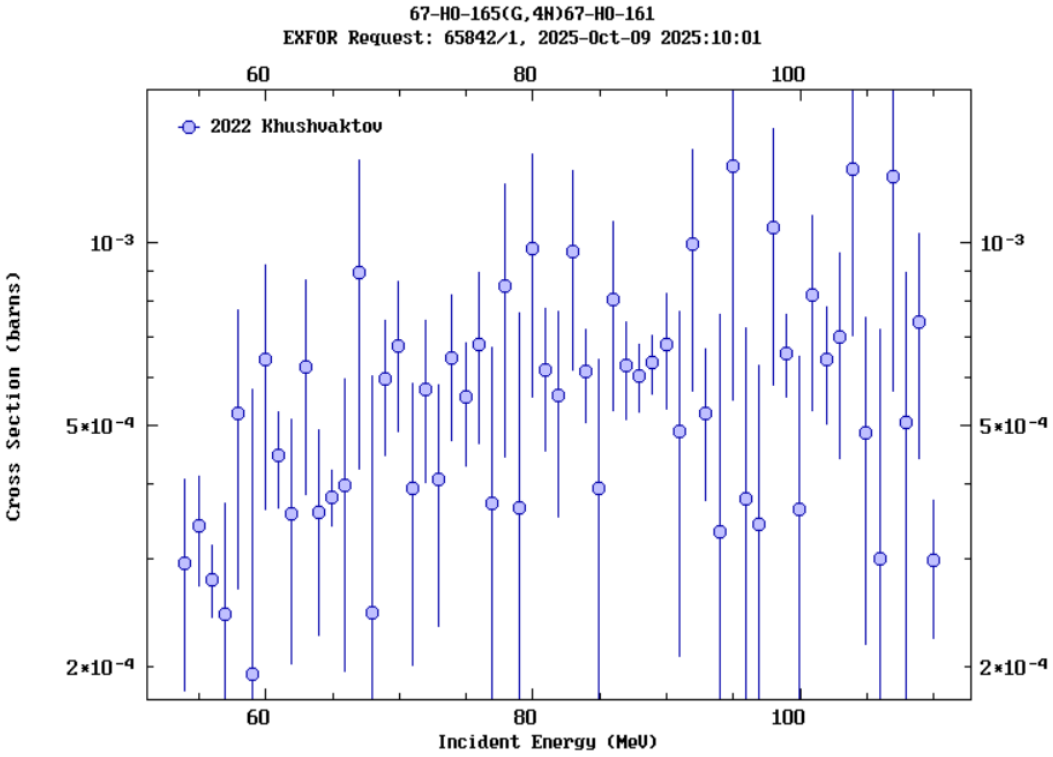

Fig. 11. EXFOR data for the ^{165}Ho(γ,4n)^{161}Ho reaction. Reaction cross sections as a function of energy [5]

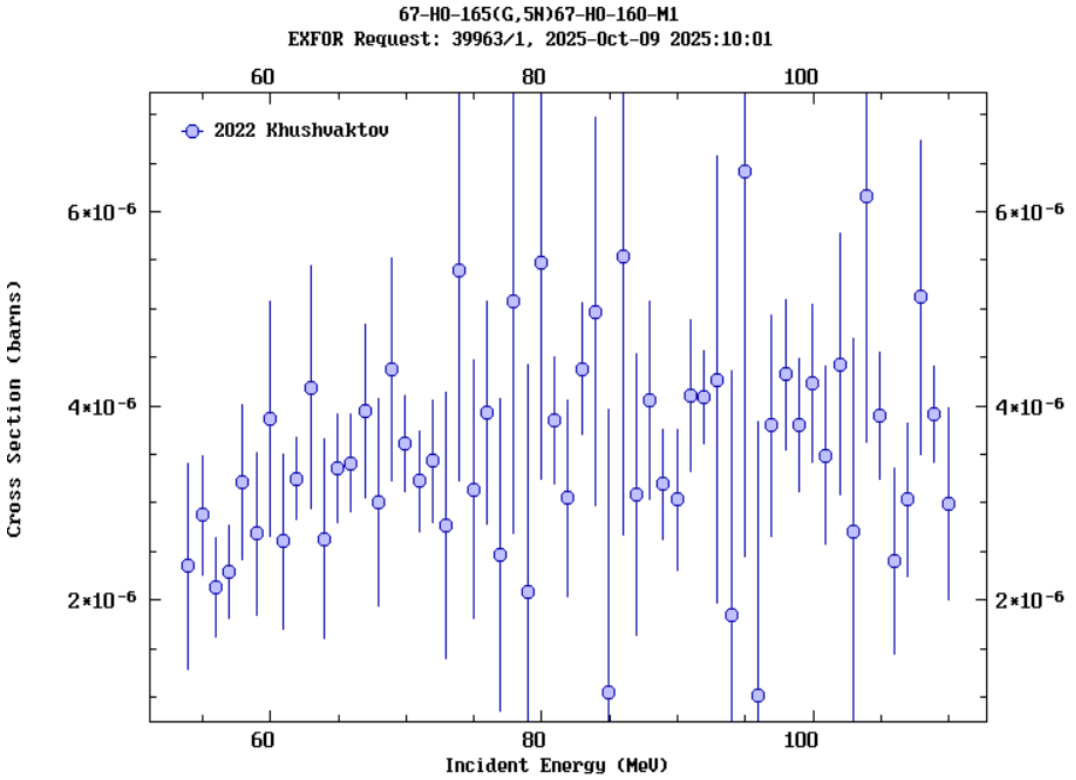

Fig. 12. EXFOR data for the 165Ho(γ,5n)160Ho reaction. Reaction cross sections as a function of energy [5].

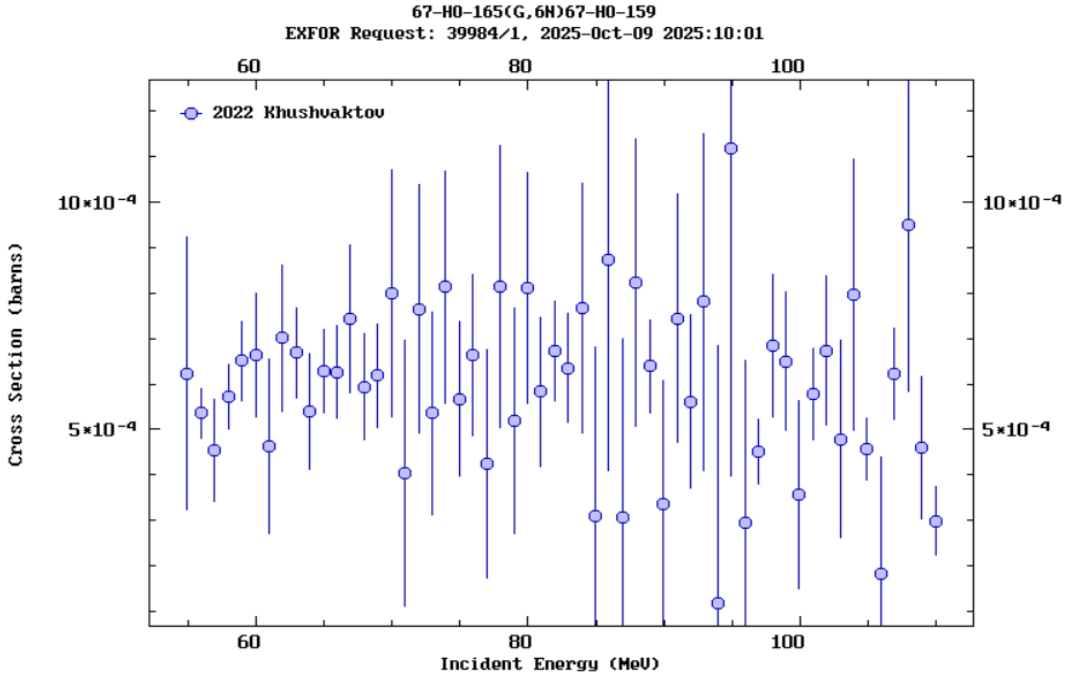

Fig. 13. EXFOR data for the 165Ho(γ,5n)159Ho reaction. Reaction cross sections as a function of energy [5].

The **absolute reaction yield (rate)** was determined based on the experimental data using the following formula:

$$R_{exp} = \frac{S_p \cdot C_{abs}}{\varepsilon_p \cdot I_\gamma} \frac{t_{real}}{t_{live}} \frac{1}{N} \frac{1}{N_e - 1} \frac{e^{\lambda \cdot t_{cool}}}{1 - e^{-\lambda \cdot t_{real}}} \frac{\lambda \cdot t_{irr}}{1 - e^{-\lambda \cdot t_{irr}}} \qquad (4)$$

t_{live}- live time (the time during which the detector actually recorded signals, excluding dead time);

ε_p- efficiency of the detector for the full-energy peak;

I_γ - gamma-ray emission probability, i.e., the probability of gamma emission per decay;

t_{cool}- cooling time (time elapsed between the end of irradiation and the start of measurement);

t_{irr}- irradiation time;

N_{e^-}- total number of electrons reaching the converter (integrated number);

N- number of target (activatable) atoms in the sample;

λ - radioactive decay constant.

In our study, the same formula for the **absolute reaction yield** was used to determine the **experimental relative reaction yields**. As the experimental relative reaction yield, the yield of all photonuclear reactions was normalized to the (γ,n) reaction yield.

For calculations, the following formula for the **relative reaction yield** was used:

$$Y_{rel,i} = \frac{\int_{E_{th}}^{E_{\gamma max}} \sigma_i(E)\, W(E, E_{\gamma max})\, dE}{\int_{E_{th}}^{E_{\gamma max}} \sigma_{(\gamma,n)}(E)\, W(E, E_{\gamma max})\, dE} \quad (5)$$

For calculating the **flux-averaged cross section**, the following formula was used:

$$\langle \sigma \rangle = \frac{\int_{E_{th}}^{E_{\gamma max}} \sigma_i(E)\, W(E, E_{\gamma max})\, dE}{\int_{E_{th}}^{E_{\gamma max}} W(E, E_{\gamma max})\, dE} \quad (6)$$

$\sigma_i(E)$ - energy-dependent cross section of the iii-th reaction (reaction probability);

$W(E,E_{\gamma max})$ - energy distribution or "flux" of photons in the bremsstrahlung radiation;

E_{th} - threshold energy of the reaction;

$E_{\gamma max}$ - maximum photon energy.

For calculating the **flux-averaged cross section** from the experiment, instead of using the number of electrons reaching the converter N_{e^-} in the reaction yield formula, the **number of photons incident on the Ho sample with energies above the reaction threshold** was used.

Results and Discussions

3.1. Calculated Relative Yields of Photonuclear Reactions in ^{165}Ho and Their Comparison with Experimental Results

In this section, the **relative reaction yields** of various photonuclear reaction channels produced in ^{165}Ho nuclei are calculated and presented in graphs (Figures 15, 16, 17, 18, 19, 20). During the study, using the **Geant4 simulation toolkit**, electron beams with energies in the range of 50–110 MeV (increasing in 5 MeV steps) were simulated, and separate calculations were performed for **3 mm and 5 mm thick lead converters**, modeling the entire process. In addition, **proton-emission reactions**, namely ^{165}Ho(γ,3p3n)^{159}Gd and ^{165}Ho(γ,7n2p)^{156}Tb, were analyzed using Geant4, and their relative reaction yields were calculated. When compared with experimental data, noticeable discrepancies appeared, which can be seen in **Figures 19–20**.

To study this in more detail, for the ^{165}Ho(γ,7n2p)^{156}Tb proton-emission reaction, the **reaction cross sections** of the resulting ^{156}Tb were calculated separately using Geant4 and TALYS, and the relative yields were plotted and compared with experimental results **(Fig. 20)**. Even in this comparison, differences between Geant4, TALYS, and experimental results were observed.

This shows that Geant4 and TALYS **accurately model simple γ–nucleus reactions**, but proton-emission reactions are more complex and do not fully agree with experimental data. This indicates **limitations in the physics modules of Geant4 and TALYS for calculating proton-emission reaction channels**.

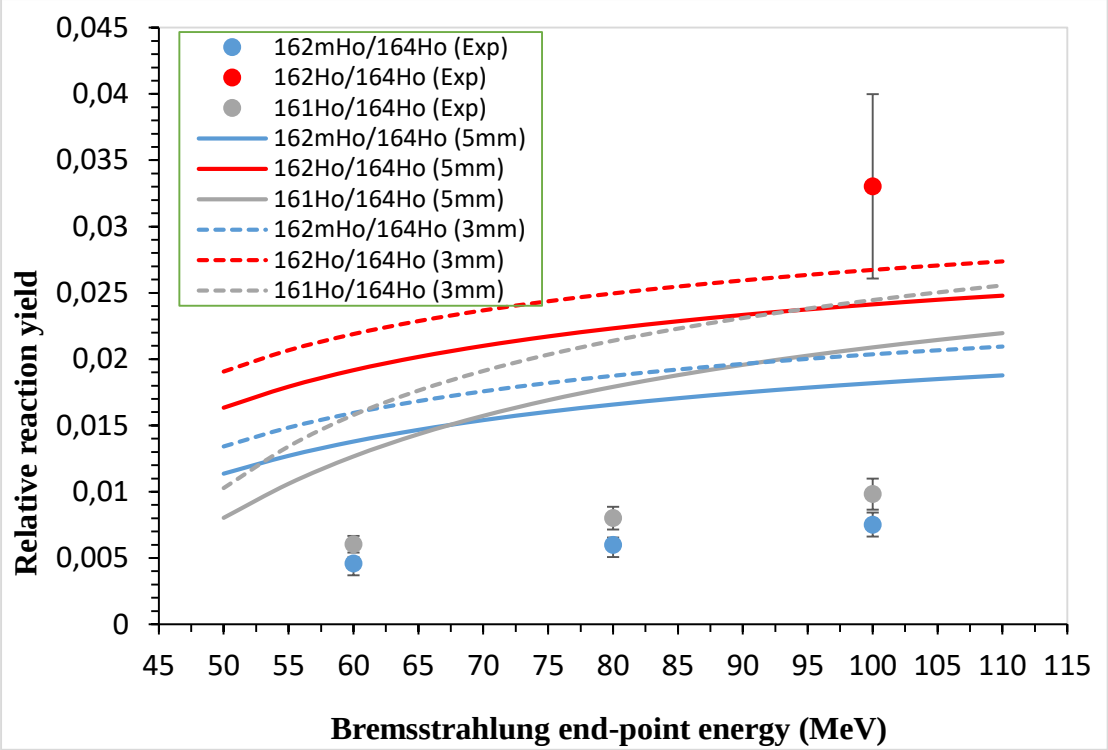

Fig. 14. Relative reaction yields of ^{162m}Ho, ^{162}Ho, and ^{161}Ho produced in the ^{165}Ho(γ,3n)^{162m}Ho, ^{165}Ho(γ,3n)^{162}Ho, and ^{165}Ho(γ,4n)^{161}Ho reactions, calculated using Geant4, along with experimental results for comparison.

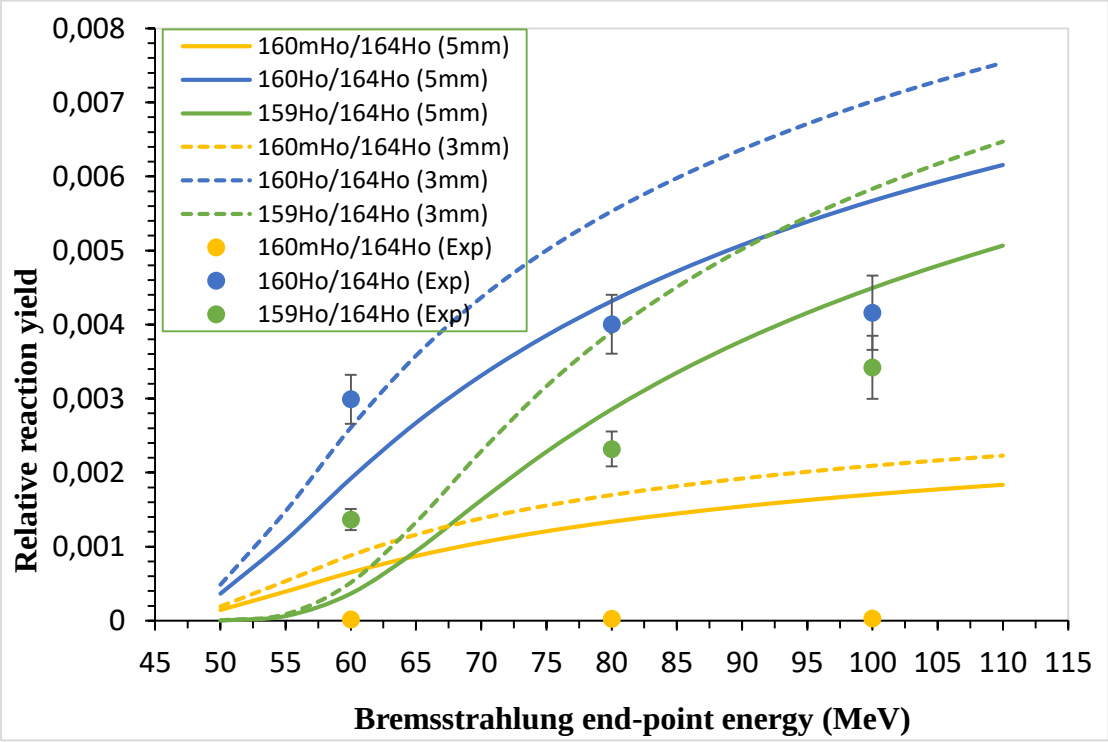

Fig. 15. Relative reaction yields of ^{160m}Ho, ^{160}Ho, and ^{159}Ho produced in the ^{165}Ho(γ,5n)^{160m}Ho, ^{165}Ho(γ,5n)^{160}Ho, and ^{165}Ho(γ,6n)^{159}Ho reactions, calculated using Geant4, along with experimental results for comparison.

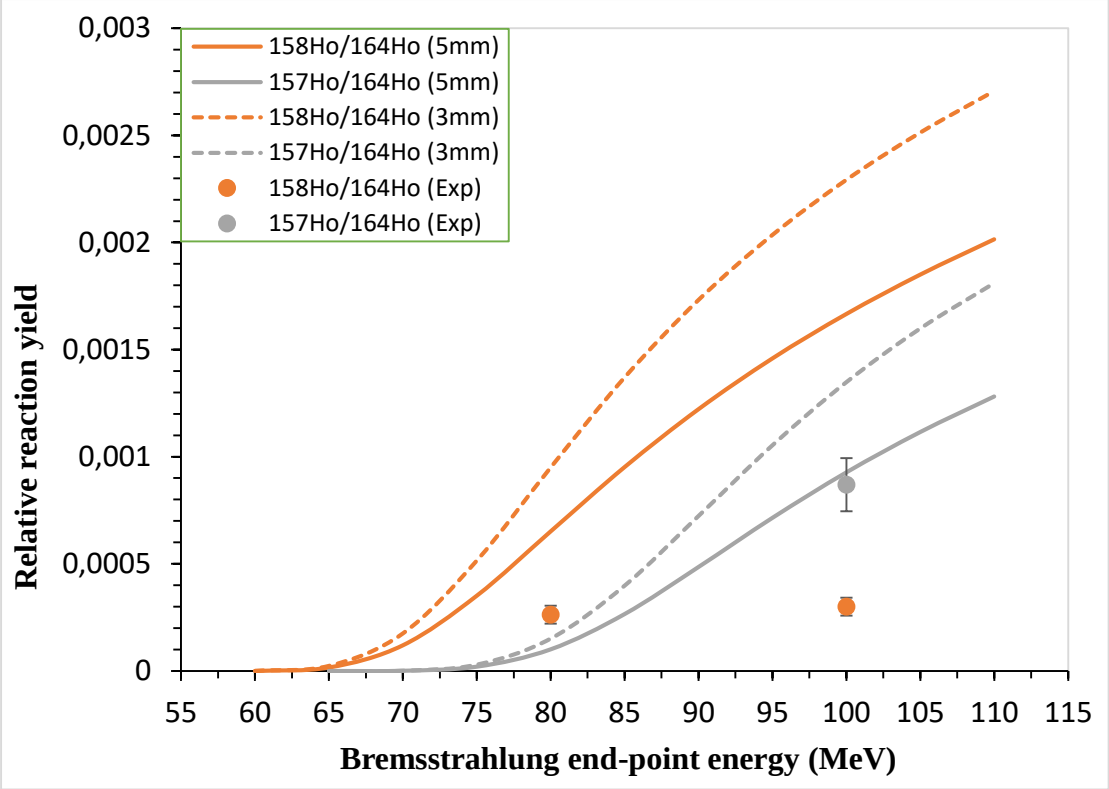

Fig. 16. Relative reaction yields of ^{158}Ho and ^{157}Ho produced in the ^{165}Ho(γ,7n)^{158}Ho and ^{165}Ho(γ,8n)^{157}Ho reactions, calculated using Geant4.

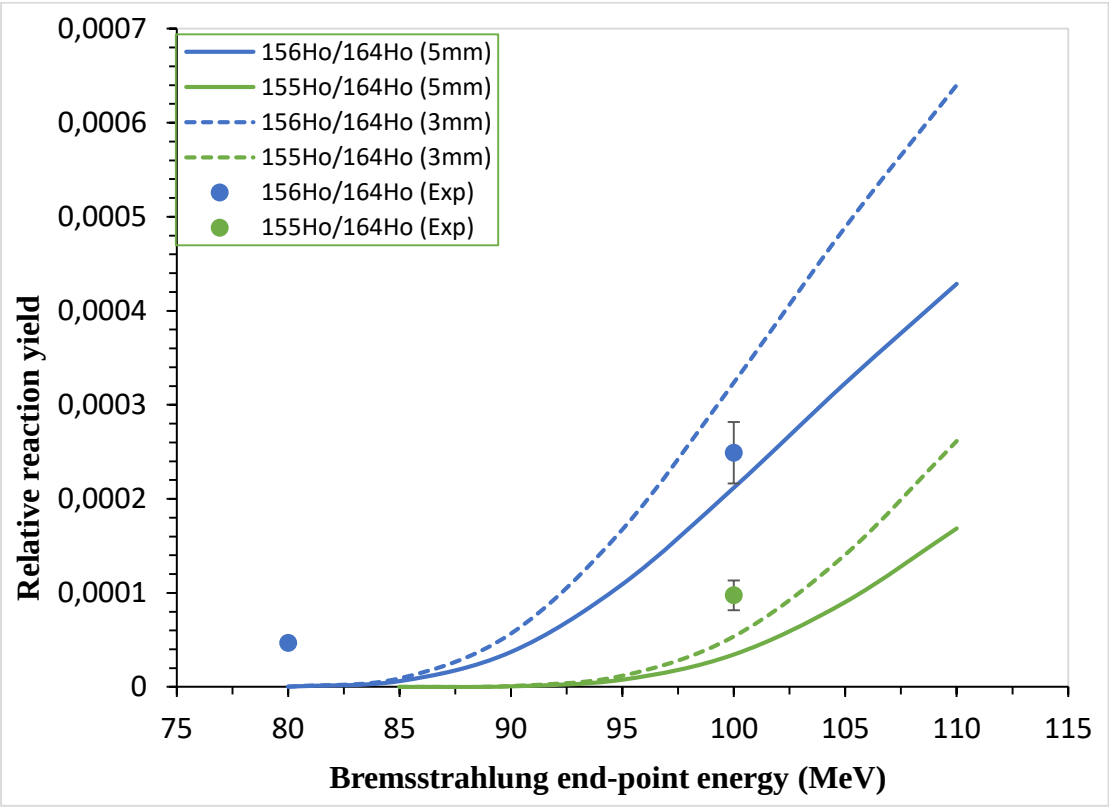

Fig. 17. Relative reaction yields of ^{156}Ho and ^{155}Ho produced in the ^{165}Ho(γ,9n)^{156}Ho and ^{165}Ho(γ,10n)^{155}Ho reactions, calculated using Geant4, along with experimental results for comparison.

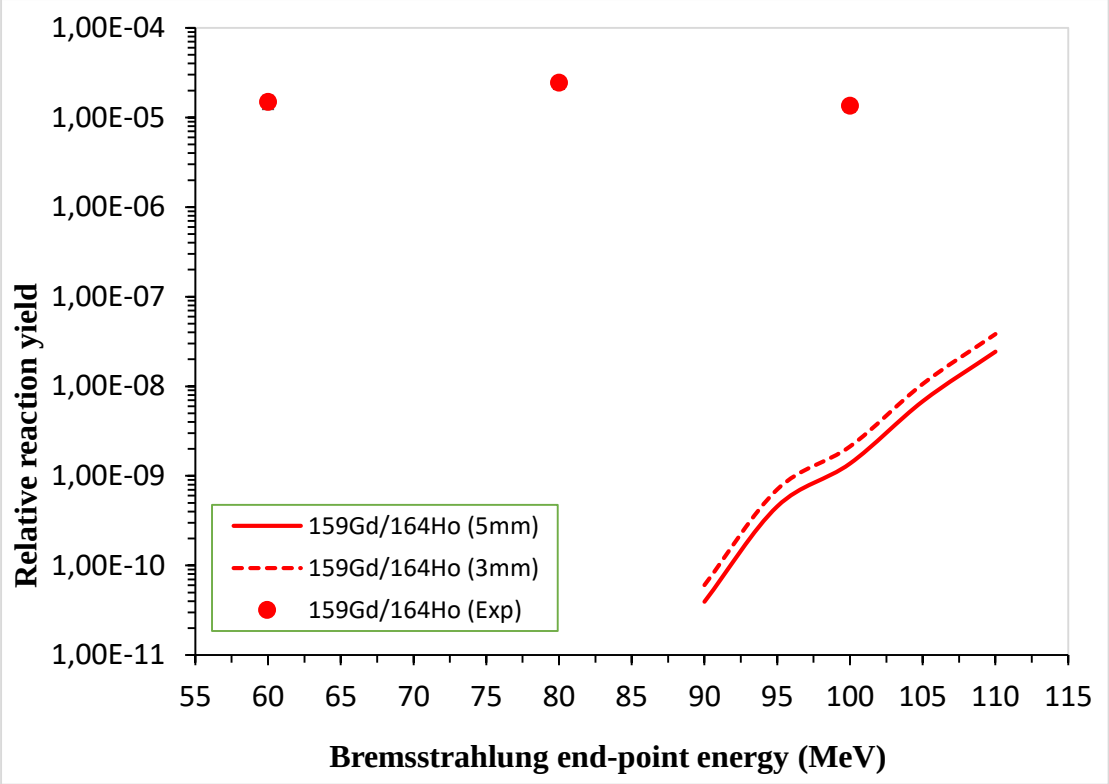

Fig. 18. Relative reaction yield of ^{159}Gd produced in the ^{165}Ho(γ,3p3n)^{159}Gd reaction, calculated using Geant4, along with experimental results for comparison.

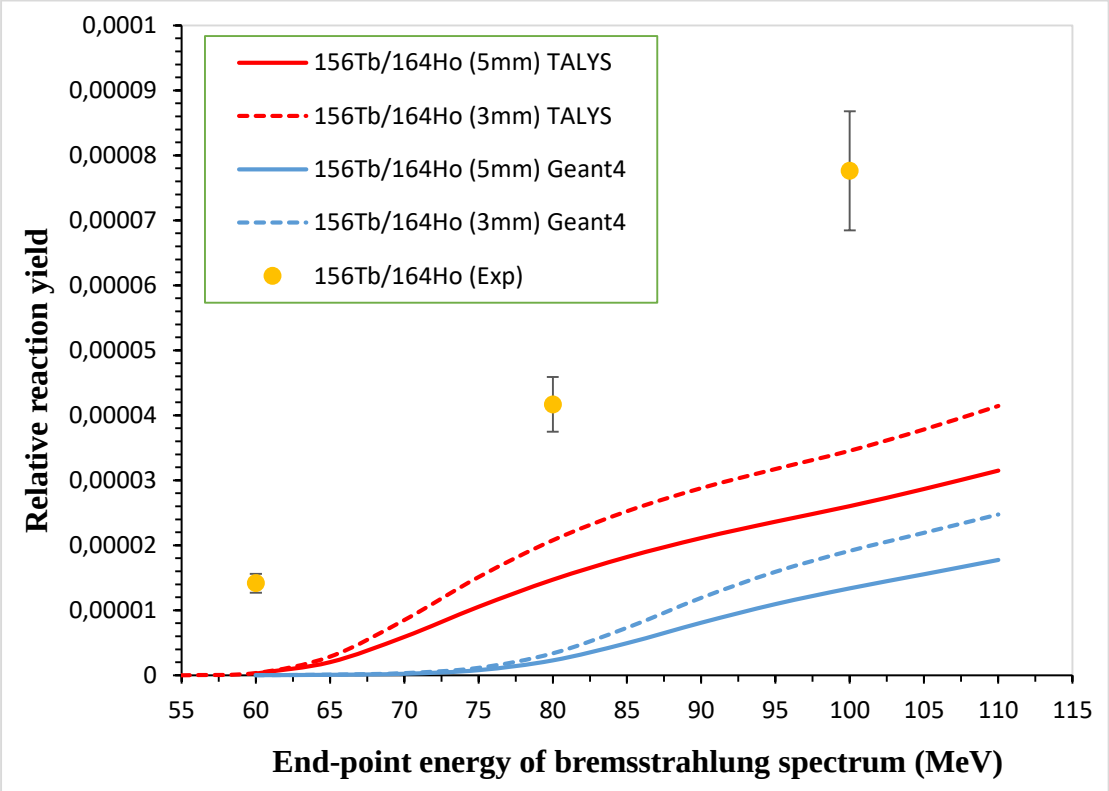

Fig. 19. Reaction cross sections of ^{156}Tb calculated using TALYS and Geant4 (for 3 mm and 5 mm converters) and relative reaction yields for ^{165}Ho(γ,7n2p)^{156}Tb, along with a comparison to the relative reaction yields obtained experimentally.

3.2. Calculated Flux-Averaged Cross Sections of Photonuclear Reactions and Their Comparison with Experimental Results

In this section, the **calculated flux-averaged cross sections** (⟨σ⟩) for photonuclear reactions in ^{165}Ho are presented and analyzed in graphs (**Figures 21, 22, 23, 23, 24, 25, 26, 27, 28, 29, 30, 31, 32, 33**). The study was conducted using the **Geant4 simulation toolkit** for modeling these processes.

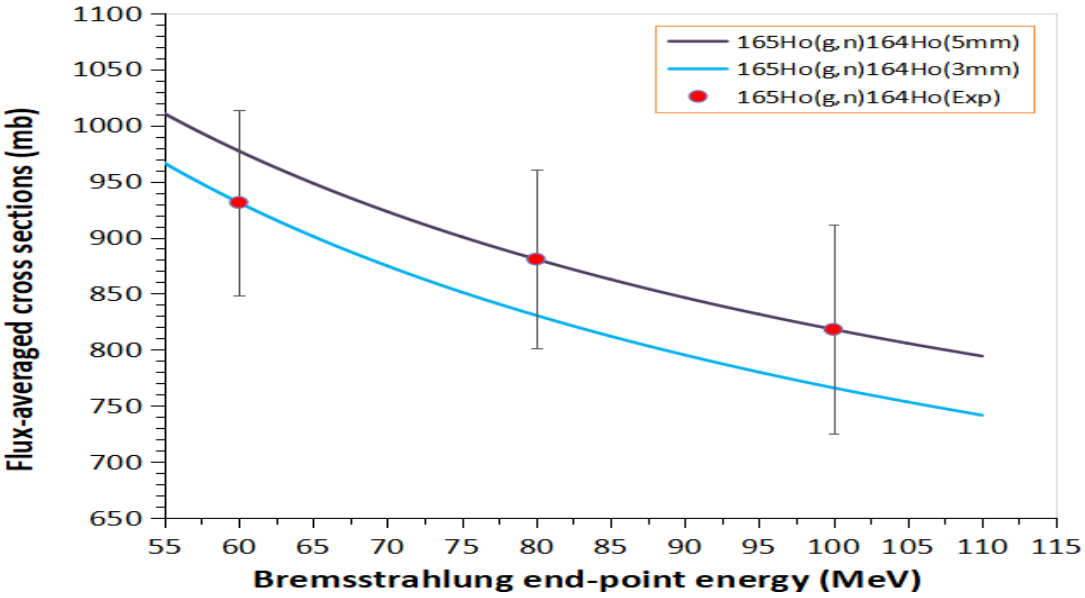

Fig. 20. Flux-averaged cross section calculated using Geant4 for ^{164}Ho produced in the ^{165}Ho(γ,n)^{164}Ho reaction.

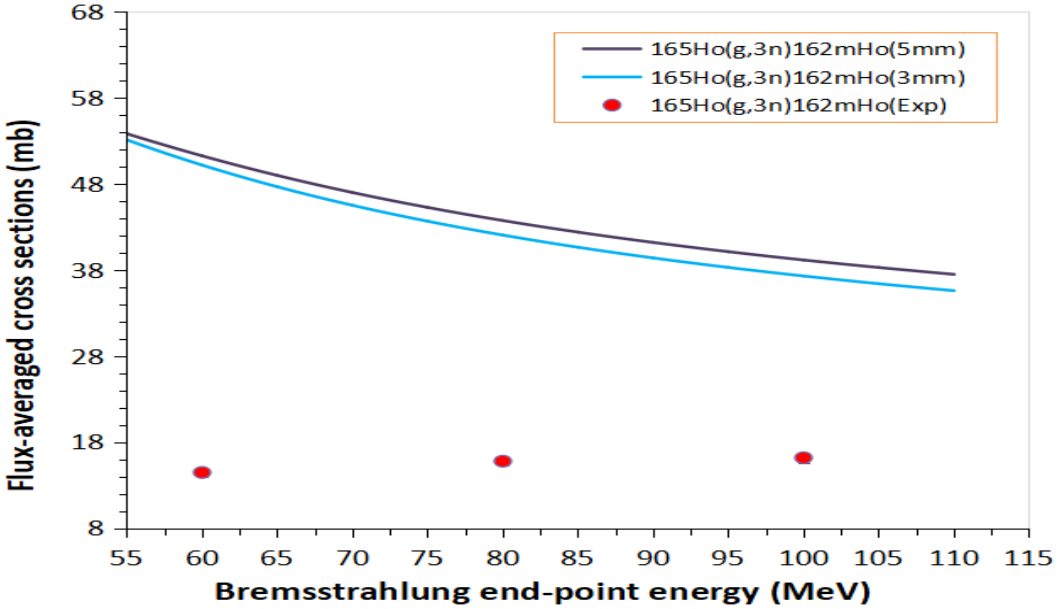

Fig. 21. Flux-averaged cross section calculated using Geant4 for ^{162m}Ho produced in the ^{165}Ho(γ,3n)^{162m}Ho reaction.

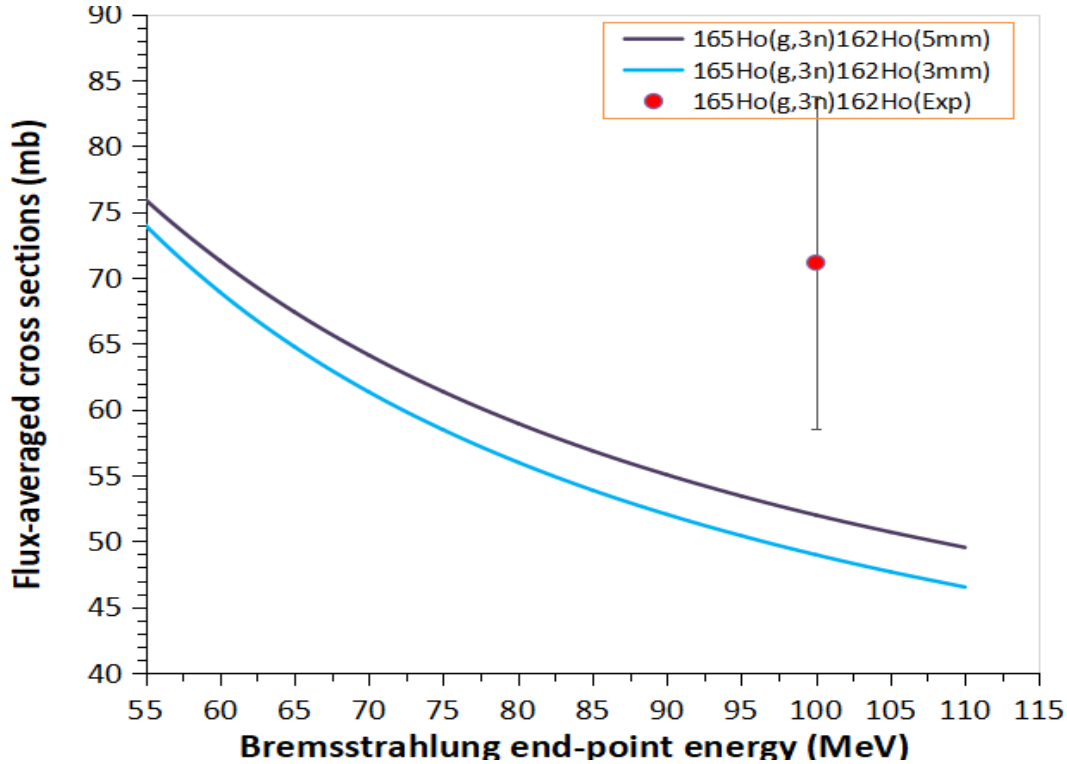

Fig. 22. Flux-averaged cross section calculated using Geant4 for ^{162}Ho produced in the ^{165}Ho(γ,n)^{162}Ho reaction.

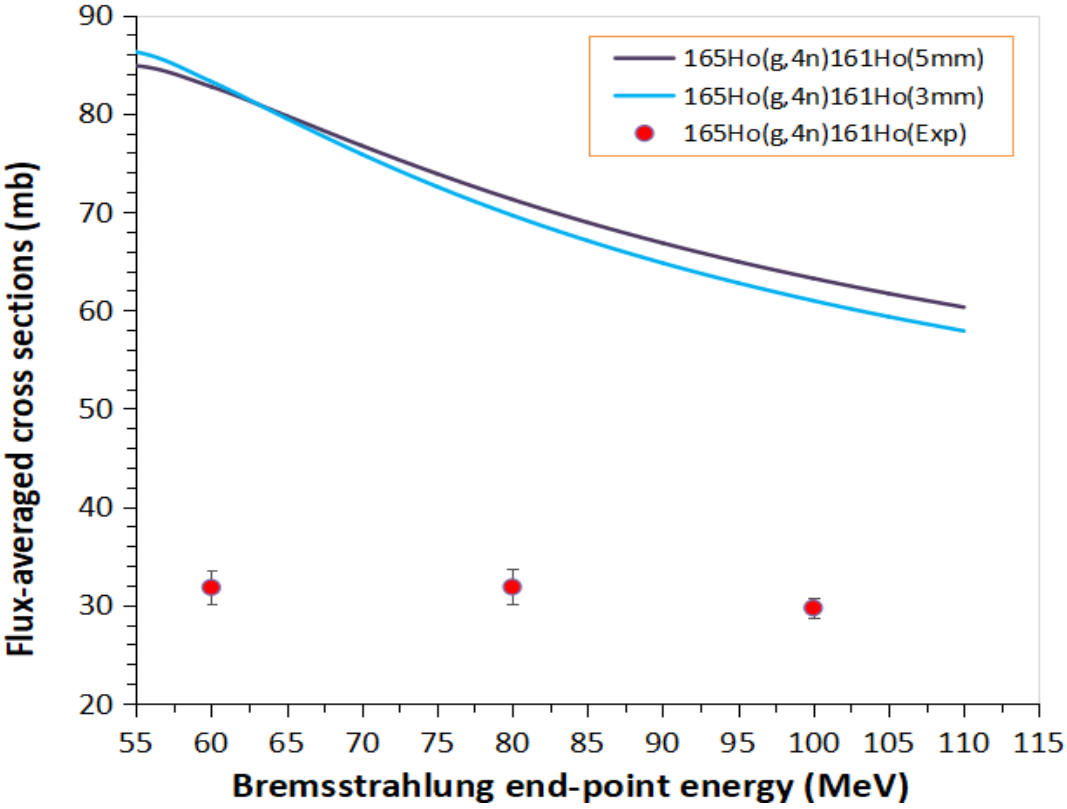

Fig. 23. Flux-averaged cross section calculated using Geant4 for ^{161}Ho produced in the ^{165}Ho(γ,4n)^{161}Ho reaction.

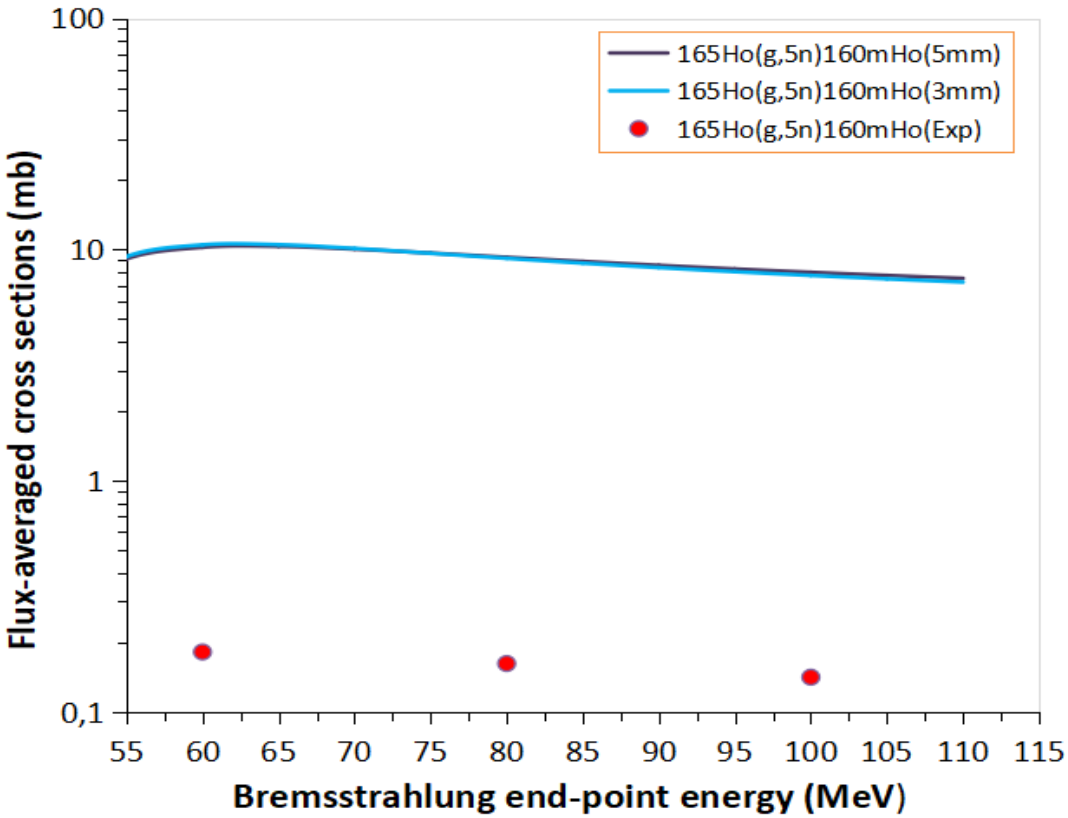

Fig. 24. Flux-averaged cross section calculated using Geant4 for ^{160m}Ho produced in the ^{165}Ho(γ,5n)^{160m}Ho reaction.

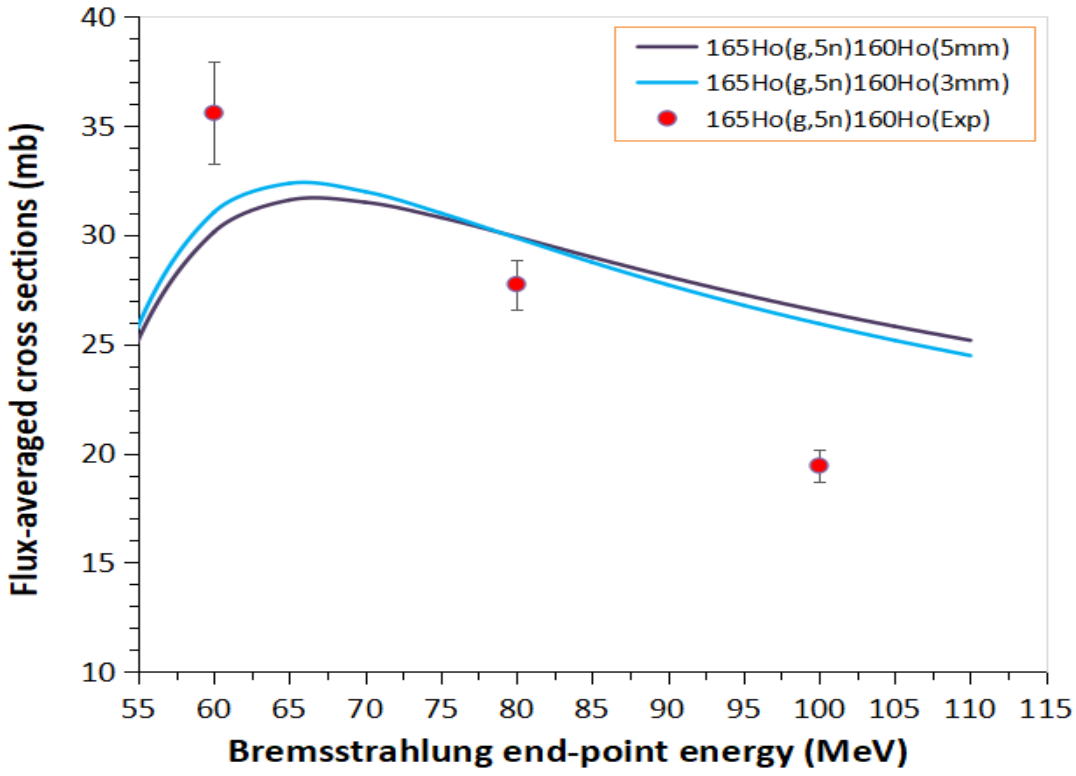

Fig. 25. Flux-averaged cross section calculated using Geant4 for ^{160}Ho produced in the ^{165}Ho(γ,5n)^{160}Ho reaction.

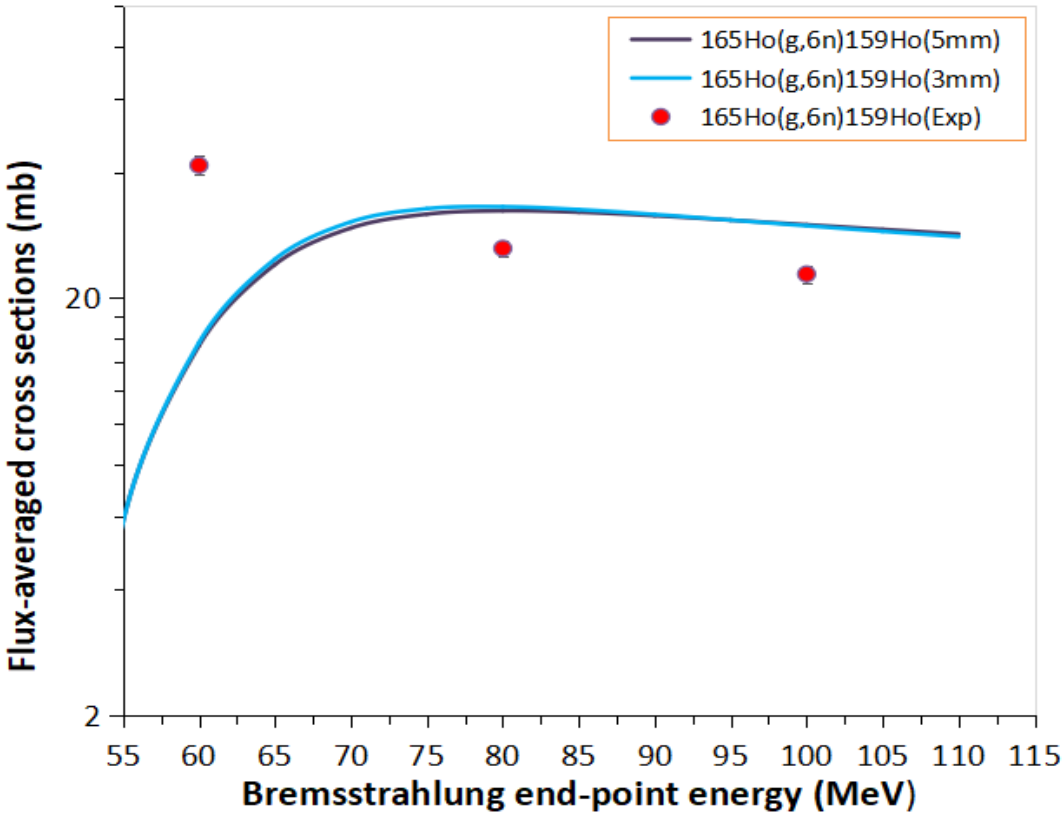

Fig. 26. Flux-averaged cross section calculated using Geant4 for ^{159}Ho produced in the ^{165}Ho(γ,6n)^{159}Ho reaction.

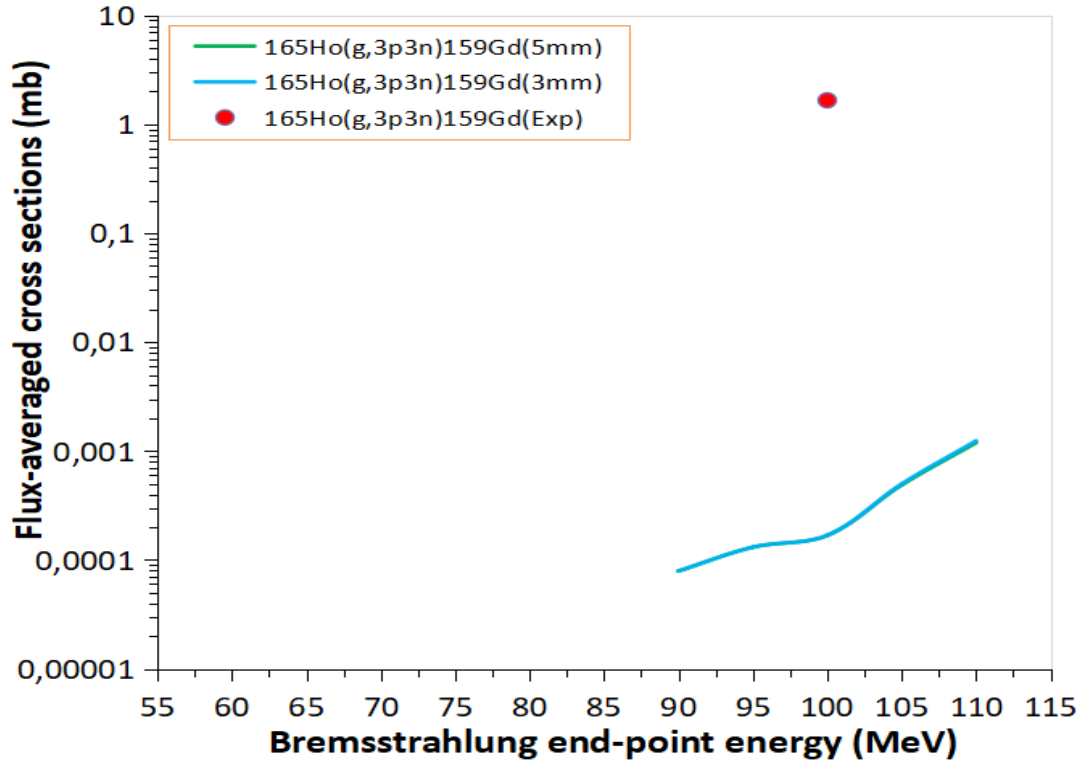

Fig. 27. Flux-averaged cross section calculated using Geant4 for ^{159}Gd produced in the ^{165}Ho(γ,3p3n)^{159}Gd reaction.

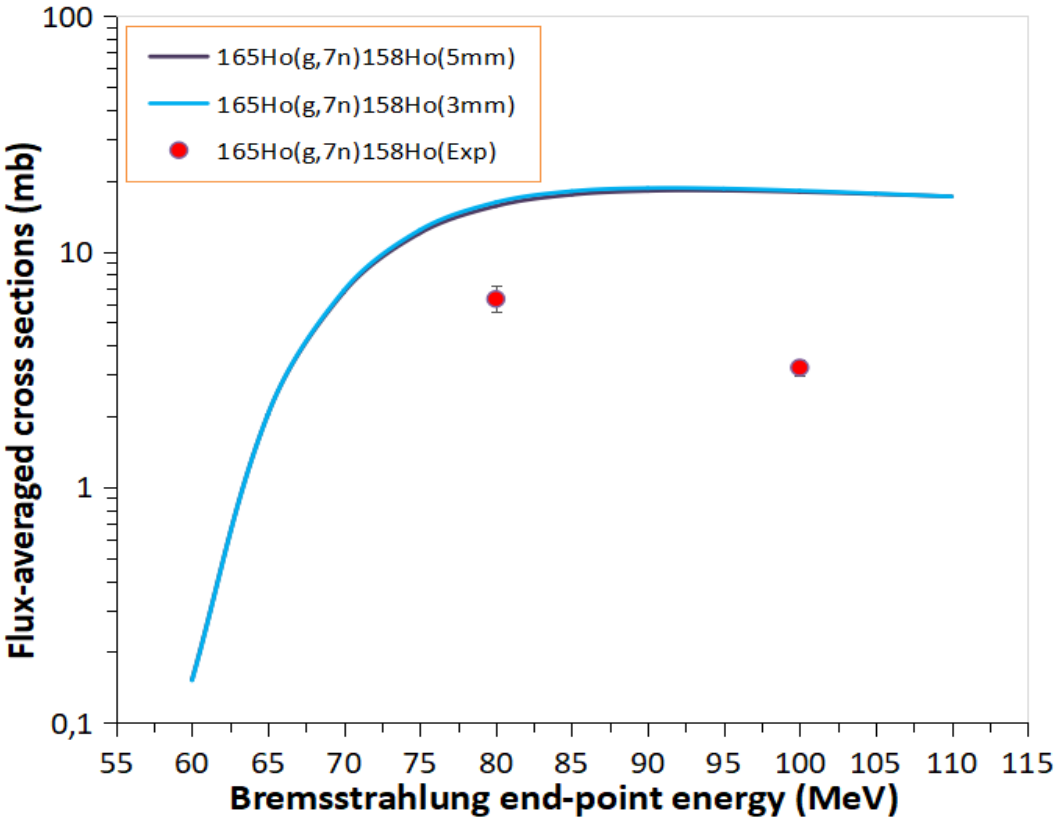

Fig. 28. Flux-averaged cross section calculated using Geant4 for ^{158}Ho produced in the ^{165}Ho(γ,7n)^{158}Ho reaction.

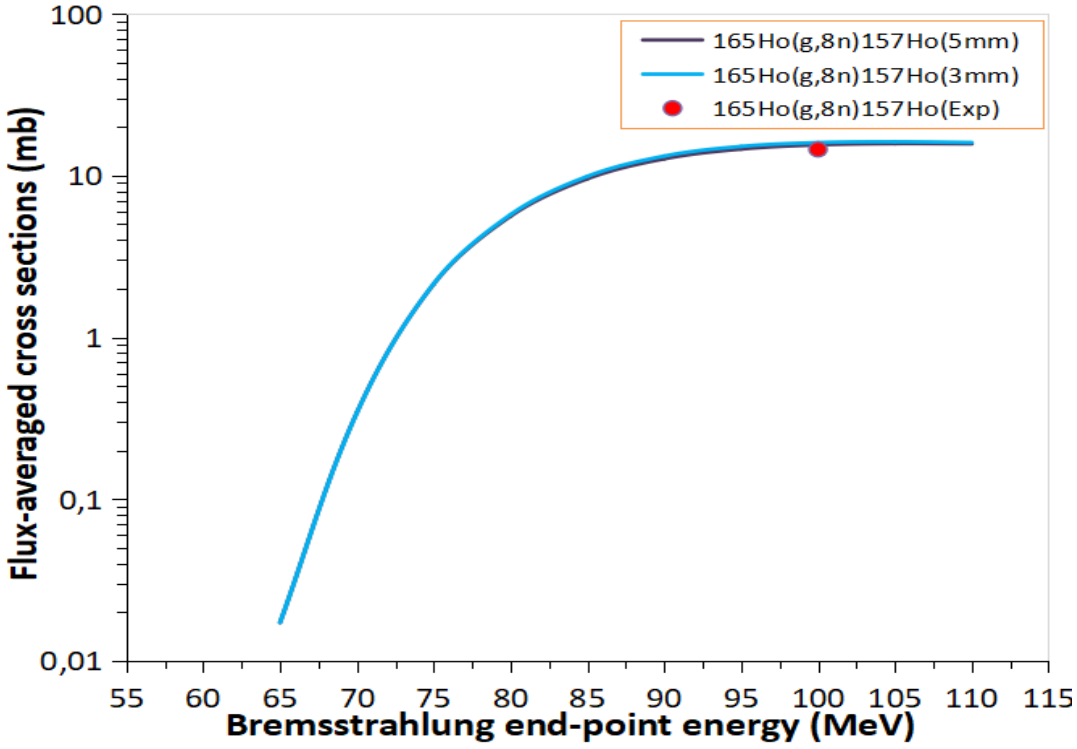

Fig. 29. Flux-averaged cross section calculated using Geant4 for ^{157}Ho produced in the ^{165}Ho(γ,8n)^{157}Ho reaction.

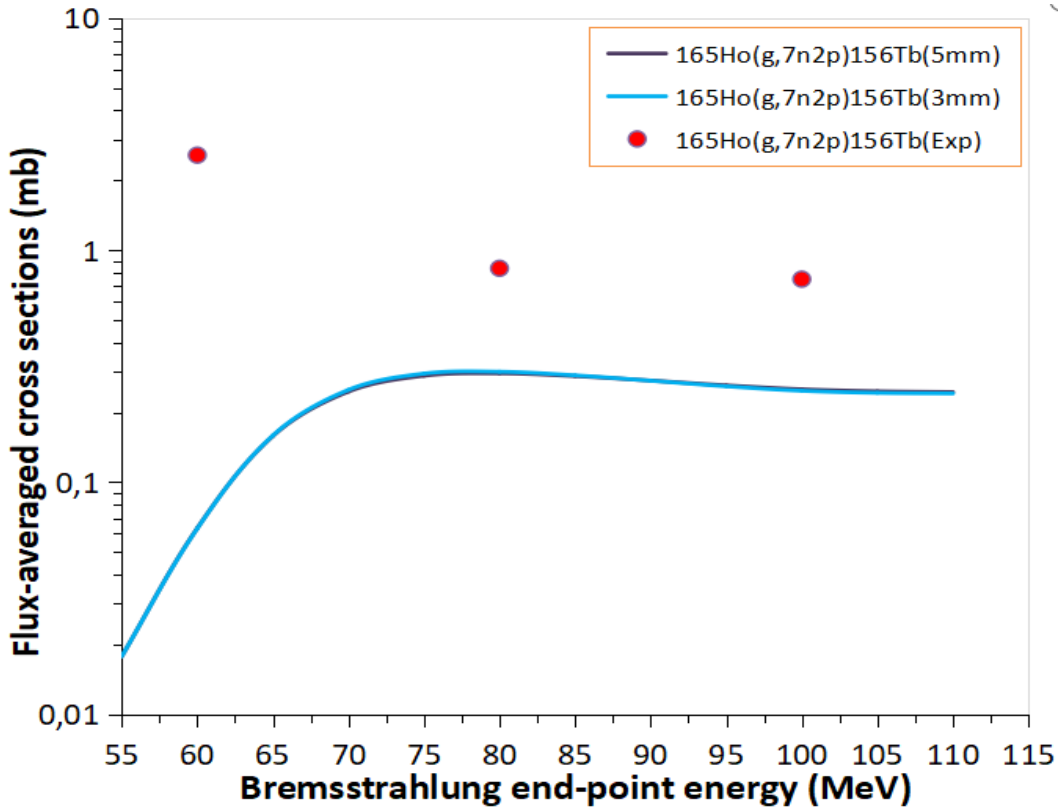

Fig. 30. Flux-averaged cross section calculated using Geant4 for ^{156}Tb produced in the ^{165}Ho(γ,7n2pn)^{156}Tb reaction.

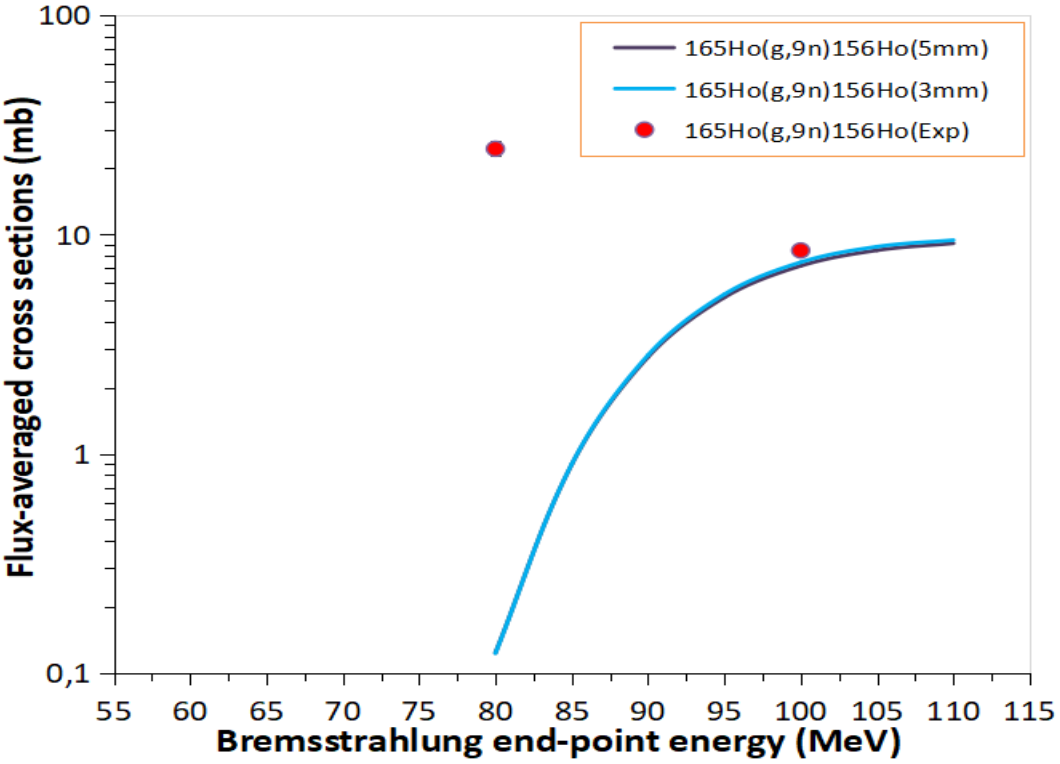

Fig. 31. Flux-averaged cross section calculated using Geant4 for ^{156}Ho produced in the ^{165}Ho(γ,9n)^{156}Ho reaction.

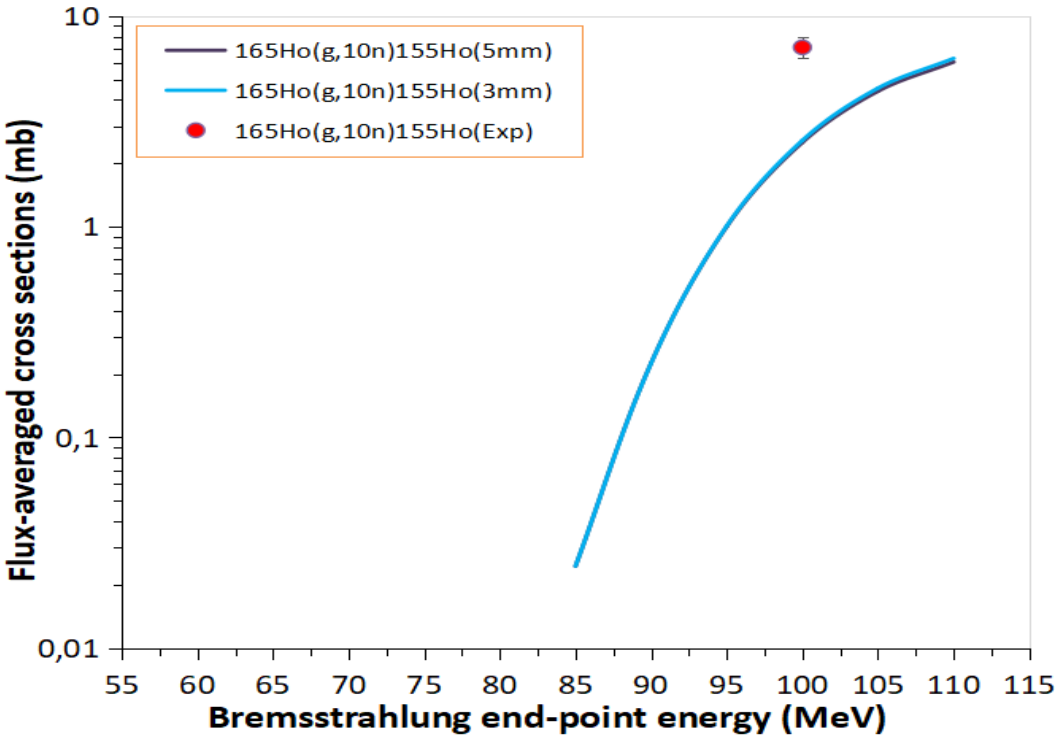

Fig. 32. Flux-averaged cross section calculated using Geant4 for ^{155}Ho produced in the ^{165}Ho(γ,10n)^{155}Ho reaction.

Conclusion

In conclusion, in this study, using the **Geant4** and **TALYS** programs, the **relative reaction yields** and **flux-averaged cross sections** of reaction channels produced in ^{165}Ho nuclei were determined. Furthermore, the combined use of Geant4 and TALYS provides an effective approach for studying photonuclear reactions. However, limitations of the Geant4 and TALYS models become apparent when modeling **proton-emission reactions** and calculating the corresponding reaction channels. Therefore, in future studies of photonuclear reactions, the research can be further improved by employing additional software packages alongside these tools. Additionally, for investigations involving proton-emission reactions, it is recommended to enhance these programs to more accurately calculate the physical parameters of the reaction channels.

References

1. http://flnph.jinr.ru/ru/facilities/iren.

2. https://ec.europa.eu/jrc/en/research-facility/linearelectron-accelerator-facility.

3. www.phy.ornl.gov/nuclear/orela/.

4. J. H. Khushvaktov et al., Phys. Part. Nucl. Lett. **17**, 821-822-823 (2020).

5. J. H. Khushvaktov et al., Phys. Part. Nucl. Lett. **19**, 347 (2022).

6. https://ru.wikipedia.org/wiki/Geant4

7. https://physicsopenlab.org/2017/08/02/bremsstrahlung-radiation/

8. Учебное пособие / В.В.Варламов, Б.С.Ишханов, И.М.Капитонов – М.: Университетская книга, 2008. – 9 с.

9. B. L. Berman, M. A. Kelly, R. L. Bramblett, J. T. Cald well, H. S. Davis, and S. C. Fultz, Phys. Rev. **185**, 1576 (1969).

10. R. Bergère, H. Beil, and A. Veyssière, Nucl. Phys. A **121**, 463–480 (1968).

Acknowledgments

I would like to express my sincere gratitude to my scientific advisor, **Dr. Jurabek Khushvaktov**, for his continuous support throughout this research. During my 8-week internship, he taught me many valuable things and provided me with useful guidance and advice. I would also like to thank **Fayziev Fayzulloh** for his companionship and assistance during this period. Furthermore, I extend my special thanks to the members of the **START team** and **Elena Karpova**, as their support allowed me to undertake practical work at one of the world's leading research institutes and provided me with all the opportunities to make my internship both productive and enjoyable.